

Article

# Precessing Black Hole Binaries and Their Gravitational Radiation

László Á. Gergely \* , Zoltán Keresztes  and Márton Tápai 

Institute of Physics, University of Szeged, Dóm tér 9, H-6720 Szeged, Hungary; zkeresztes.zk@gmail.com (Z.K.); tapai.marton@gmail.com (M.T.)

\* Correspondence: laszlo.a.gergely@gmail.com;

Received: 27 November 2017 ; Accepted: 17 January 2018 ; Published: 16 February 2018

**Abstract:** The first and second observational runs of Advanced Laser Interferometer Gravitational-wave Observatory (LIGO) have marked the first direct detections of gravitational waves, either from black hole binaries or, in one case, from coalescing neutron stars. These observations opened up the era of gravitational wave astronomy, but also of gravitational wave cosmology, in the form of an independent derivation of the Hubble constant. They were equally important to prove false a plethora of modified gravity theories predicting gravitational wave propagation speed different from that of light. For a continued and improved testing of general relativity, the precise description of compact binary dynamics, not only in the final coalescence phase but also earlier, when precessional effects dominate, are required. We report on the derivation of the full secular dynamics for compact binaries, valid over the precessional time-scale, in the form of an autonomous closed system of differential equations for the set of spin angles and periastron. The system can be applied for mapping the parameter space for the occurrence of the spin flip-flop effect and for more accurately analyzing the spin-flip effect, which could explain the formation of X-shaped radio galaxies.

**Keywords:** gravitational waves; compact binary systems; post-Newtonian dynamics

## 1. Introduction

One century after Einstein first proposed the existence of gravitational waves [1], as predicted by his general theory of relativity, their direct detection by the pair of Advanced Laser Interferometer Gravitational-wave Observatory (LIGO) laser-interferometric detectors [2] has been announced [3] by the LIGO Scientific Collaboration and Virgo Collaboration. The excitement generated by this marvellous scientific achievement has been further amplified by the second [4] and the third direct detection [5] by the twin LIGO detectors. The sources were identified in all three cases to be coalescing astrophysical black hole binaries, with masses slightly higher than expected from stellar evolution. The localization of these sources was however poor, with only these two detectors being in operation at that time. This has been improved to  $60 \text{ deg}^2$  in the case of the fourth direct detection [6] of gravitational waves also generated by coalescing black hole binaries, which was signaled by the then operational Advanced Virgo detector too [7]. Moreover, a fifth event [8] has been reported, this time generated by a pair of colliding neutron stars. The low  $\text{SNR} = 2.0$  of this event in the Virgo Observatory has put stringent constraints on its sky localization, which was reduced to  $28 \text{ deg}^2$ . Although better than the localization of the source in gamma-rays, this is still far too large compared to usual localization accuracy at other frequencies in the electromagnetic spectrum, making it clear that, for reliable sky localization, more detectors are needed. In this respect the soon-to-be commissioned Kamioka Gravitational Wave Detector (KAGRA) detector [9] and the planned LIGO India [10] observatory will play important roles.

The fifth event [8] was followed after 1.7 s by the soft gamma ray burst GRB170817A from the same sky region [11] and in a few hours the source has been precisely identified in almost all

frequencies of the electromagnetic spectrum [12]. It has been confirmed that neutron star mergers are the sources of soft gamma ray bursts. The merger was followed by a kilonova explosion, producing an abundance of heavy elements. The determination of the luminosity distance from the gravitational wave measurement and of the redshift from the electromagnetic observations (although with yet large error) has led to a new way of calculating the Hubble constant [13], for which supernova IA measurements and cosmic microwave background observations led to values in slight tension.

Based on Lorentz's assumption [14] from as early as 1904 that all forces should transform under translation in the same way as electric forces in an electrostatic system, Poincaré advanced the idea a decade before general relativity was born that gravitational waves should propagate with the speed of light [15]. Indeed, this is what follows from general relativity both in the weak field limit and in the geometric optics approximation of perturbations in strong field. However, is general relativity the final theory of gravity? While for the solar system all of its predictions were spectacularly confirmed by accurate observations, on the galactic scale and beyond there is need to add roughly six times as much dark matter as baryonic matter in order to be in agreement with observations on galactic clusters and galactic rotation curves. Moreover, on a cosmological scale there is need for yet another three times as much dark energy, responsible for late-time cosmological acceleration. The numerous attempts to identify dark matter as a new type of particle (supersymmetric [16], sterile neutrino [17], weakly interacting massive particle (WIMP) [18], axion [19]) or extra-dimensional effect [20] or massive compact halo objects (MACHOs) [21] turned out to be unsuccessful. Therefore, modified gravity models were advanced in order to eliminate the need for exotic particles. In some of these more exotic theories the gravitational waves would propagate with a velocity different from the speed of light [22]. Such theories were proven false by the direct observations of gravitational waves, either (i) based on the models of soft gamma ray production by neutron star mergers and the detected time difference of 1.7 s between GW170817 and the subsequent gamma ray burst GRB170817A [11]; or (ii) considering a hypothetical massive-graviton theory and determining the corresponding Compton-wavelength by constraining the magnitude of the related 1PN phase term [23]; or (iii) considering a dispersion relation allowing for local Lorentz-invariance violation, and as a particular subcase, for graviton mass [5]. Many modified gravity theories, however, still survived and among the ways to either confirm or falsify them, continued rigorous gravitational wave observations could have a leading role.

Given that all detections of gravitational waves were sourced by coalescing compact binary systems, it is of uttermost importance to accurately describe their evolution, both in general relativity and in modified gravity theories. In the gravitational wave dominated dissipative regime the evolution can be divided into the inspiral, merger and ringdown phase. The precise understanding of the entire evolution is desired both for understanding the details of the inspiral process and for working out predictions for future detectors.

In this paper we summarize our work done in investigating compact binary dynamics in the inspiral regime in the framework of general relativity. This process is characterized by three time-scales. The shortest is the orbital time-scale, during which the binary evolution undergoes one radial period. This might only slightly differ from a Keplerian orbit in the weak-field regime. The respective dynamics has been discussed in detail, first by including the post-Newtonian (PN) effects [24], then by inclusion of the spin-orbit (SO) and spin-spin (SS) effects [25–30], of the mass quadrupole-mass monopole (QM) effect [31,32] up to 2PN orders. This dynamics has been rigorously analyzed [33,34] through a closed system of first order ordinary differential equations derived for the orbital elements of the osculating ellipse and for the angles characterizing the spin orientations with respect to the osculating orbit. Based on this a proof was given that (i) the only binary black hole configuration allowing for spin precession with equal angular velocities about a common instantaneous axis roughly aligned to the normal of the osculating orbit, is the equal mass and parallel (aligned or antialigned) spin configuration. It has been also proven that (ii) the relative angle of the spins stays constant for equal mass black holes, irrespective of their orientation, found previously in [35] (with inclusion of only SO and SS contributions) and [36] (with all relevant contributions included, but only for circular

orbits), and (iii) the special configuration of equal mass black holes with equal, but antialigned spins, both laying in the plane of motion (leading to large recoils found in numerical simulations [37,38], although the largest was found for binaries with partially aligned spins [39]) is preserved at the second post-Newtonian (2PN) level of accuracy, for generic eccentric, parabolic or hyperbolic orbits. Further, the closed system of first-order differential equations has been rewritten in a compact form, for a set of dimensionless variables encompassing both orbital elements and spin angles, and a consistency check run to prove that the constraints are preserved during evolution [40]. As an application, the existence of a new type of interesting orbit, the chameleon orbit, has been shown, whose local, orbital parameters evolve from elliptic near pericenter, towards hyperbolic at large distances [40].

On a much larger timescale the precessional evolutions [41,42] of the spin vectors of the compact objects and of the orbital angular momentum dominate. Physical processes occurring on such time-scales are easily monitored by using a simplified dynamics, encompassing equations obtained by orbital averaging methods. These precessional evolutions were averaged for circular orbits including the SO and SS terms [35]; also for eccentric orbits with SO terms [27,28], SS terms [30], QM terms [32] included. The averaged angular dynamics has been integrated exactly for black hole binaries (assuming quadrupole parameters  $w_i = 1$ ) on circular orbits in [36], where a new constant of motion was also identified. More recently a full multi-timescale analysis was performed in [43,44], where the motion was averaged on both the orbital and the inspiral timescales. These efforts were exploited in [45] to build waveforms.

The most comprehensive instantaneous, 2PN accurate non-circular dynamics with generic quadrupole parameters discussed in [40] with consistency condition checked and the number of independent variables identified has been orbit averaged in the eccentric case [46]. In this conference presentation we succinctly summarize these secular dynamics and indicate possible applications.

## 2. Secular Dynamics and Spin Flip-Flop

The dynamics up to 2PN orders, including the SO, SS and QM couplings of compact binaries in terms of dimensionless osculating orbital elements and spin angles is given by Equations (36)–(42) of [40]. The two dimensionless shape variables characterizing the orbits of the object with reduced mass  $\mu$  moving around another body having total mass  $m$  are introduced by

$$l_r = \frac{cL_N}{Gm\mu}, \tag{1}$$

and

$$e_r = \frac{A_N}{Gm\mu}, \tag{2}$$

the latter being the eccentricity. Here,  $c$  is the speed of light,  $G$  is the gravitational constant,  $L_N$  and  $A_N$  are the magnitudes of the orbital angular momentum vector  $\mathbf{L}_N$  and Laplace–Runge–Lenz vector  $\mathbf{A}_N$ , respectively. The next set of orbital elements are the Euler angles, i.e., the inclination:

$$\alpha = \arccos(\hat{\mathbf{J}} \cdot \hat{\mathbf{L}}_N), \tag{3}$$

the longitude of the ascending node:

$$-\phi_n = \arccos(\hat{\mathbf{x}} \cdot \hat{\mathbf{1}}), \tag{4}$$

and the argument of the periastron:

$$\psi_p = \arccos(\hat{\mathbf{1}} \cdot \hat{\mathbf{A}}_N), \tag{5}$$

where  $\mathbf{J}$  is the total angular momentum including contributions from  $\mathbf{L}_N$  and from the spins  $\mathbf{S}_{1,2}$ , the hat denotes unit vectors and we have introduced  $\hat{\mathbf{I}} = \hat{\mathbf{L}}_N \times \hat{\mathbf{J}}$  and a constant unit vector  $\hat{\mathbf{x}}$  perpendicular to  $\hat{\mathbf{J}}$ . The final set required for spinning dynamics are the polar and azimuthal spin angles:

$$\kappa_i = \arccos(\hat{\mathbf{S}}_i \cdot \hat{\mathbf{L}}_N) , \tag{6}$$

$$\zeta_i = \arccos(\hat{\mathbf{S}}_i^\perp \cdot \hat{\mathbf{A}}_N) , \tag{7}$$

with  $\mathbf{S}_i^\perp = \mathbf{S}_i - \hat{\mathbf{L}}_N (\mathbf{S}_i \cdot \hat{\mathbf{L}}_N)$ . The magnitude of the spins characterized by

$$\chi_i = S_i \frac{c}{G} m_i^{-2} \tag{8}$$

is constant of motion up to 2PN orders, they occur as parameters in the evolution equations. The angles  $\alpha, \phi_n, \psi_p, \kappa_i$  and  $\psi_i = \zeta_i + \psi_p$  were represented on Figure 2 of [33].

The modulations occurring within one orbital period can be removed by averaging any function  $f$  over it:

$$T\bar{f} = \int_0^T f(t) dt = \int_0^{2\pi} f(\chi_p) \frac{1}{\dot{\chi}_p} d\chi_p . \tag{9}$$

Here, the true anomaly  $\chi_p$  is the angle between  $\mathbf{A}_N$  and the position vector of the object with reduced mass. Applying (9) for the time derivatives of  $Y = \{\bar{l}_r, e_r, \alpha, \phi_n, \psi_p, \kappa_i, \zeta_i\}$ , i.e.,  $f = \dot{Y}$ , yields the secular dynamics derived in [46]. On the secular time-scale the shape variables are constant of motion  $\bar{l}_r = \bar{e}_r = 0$ . The equations for  $\alpha, \phi_n$  and  $\kappa_i$  contain only contributions due to the SO, SS and QM couplings, while in addition to these the equations for  $\psi_p$  and  $\zeta_i$  also contain PN and 2PN relativistic terms. We give here the leading-order (PN and SO) secular contributions of the Euler angle evolutions:

$$\bar{\psi}_p^{PN} = \frac{6\pi}{\mathfrak{I} \bar{l}_r^2} , \tag{10}$$

$$\bar{\psi}_p^{SO} = -\frac{\eta\pi}{\mathfrak{I} \bar{l}_r^3} \sum_{k=1}^2 (4v^{2k-3} + 3) \chi_k [2 \cos \kappa_k + \cot \alpha \sin \kappa_k \sin(\psi_p + \zeta_k)] , \tag{11}$$

$$\bar{\alpha}^{SO} = \frac{\eta\pi}{\mathfrak{I} \bar{l}_r^3} \sum_{k=1}^2 (4v^{2k-3} + 3) \chi_k \sin \kappa_k \cos(\psi_p + \zeta_k) , \tag{12}$$

$$\bar{\phi}_n^{SO} = -\frac{\eta\pi}{\mathfrak{I} \bar{l}_r^3 \sin \alpha} \sum_{k=1}^2 (4v^{2k-3} + 3) \chi_k \sin \kappa_k \sin(\psi_p + \zeta_k) , \tag{13}$$

and of the spin angles

$$\bar{\zeta}_i^{PN} = -\bar{\psi}_p^{PN} , \tag{14}$$

$$\bar{\zeta}_i^{SO} = \frac{\eta\pi}{\mathfrak{I} \bar{l}_r^3} \{ \bar{l}_r (4 + 3v^{3-2i}) + 3 (4v^{2i-3} + 3) \chi_i \cos \kappa_i + (4v^{2j-3} + 3) \chi_j [2 \cos \kappa_j + \cot \kappa_i \sin \kappa_j \cos(\zeta_i - \zeta_j)] \} , \tag{15}$$

$$\bar{\kappa}_i^{SO} = \frac{\eta\pi}{\mathfrak{I} \bar{l}_r^3} (4v^{2j-3} + 3) \chi_j \sin \kappa_j \sin(\zeta_i - \zeta_j) . \tag{16}$$

The full set of contributions can be found in [46].

In order to ascertain the validity of the secular dynamics we compare it with the instantaneous dynamics of [40]. We depict the evolution of the nine variables under 5600 orbital periods on Figure 1. The secular and the instantaneous evolutions are shown in green and red, respectively. On the small attached figures the first two periods are also represented for better understanding. We conclude that the two dynamics follow each other on timescales which are sufficiently long as compared to the orbital period. This is a generic feature for any initial parameters.

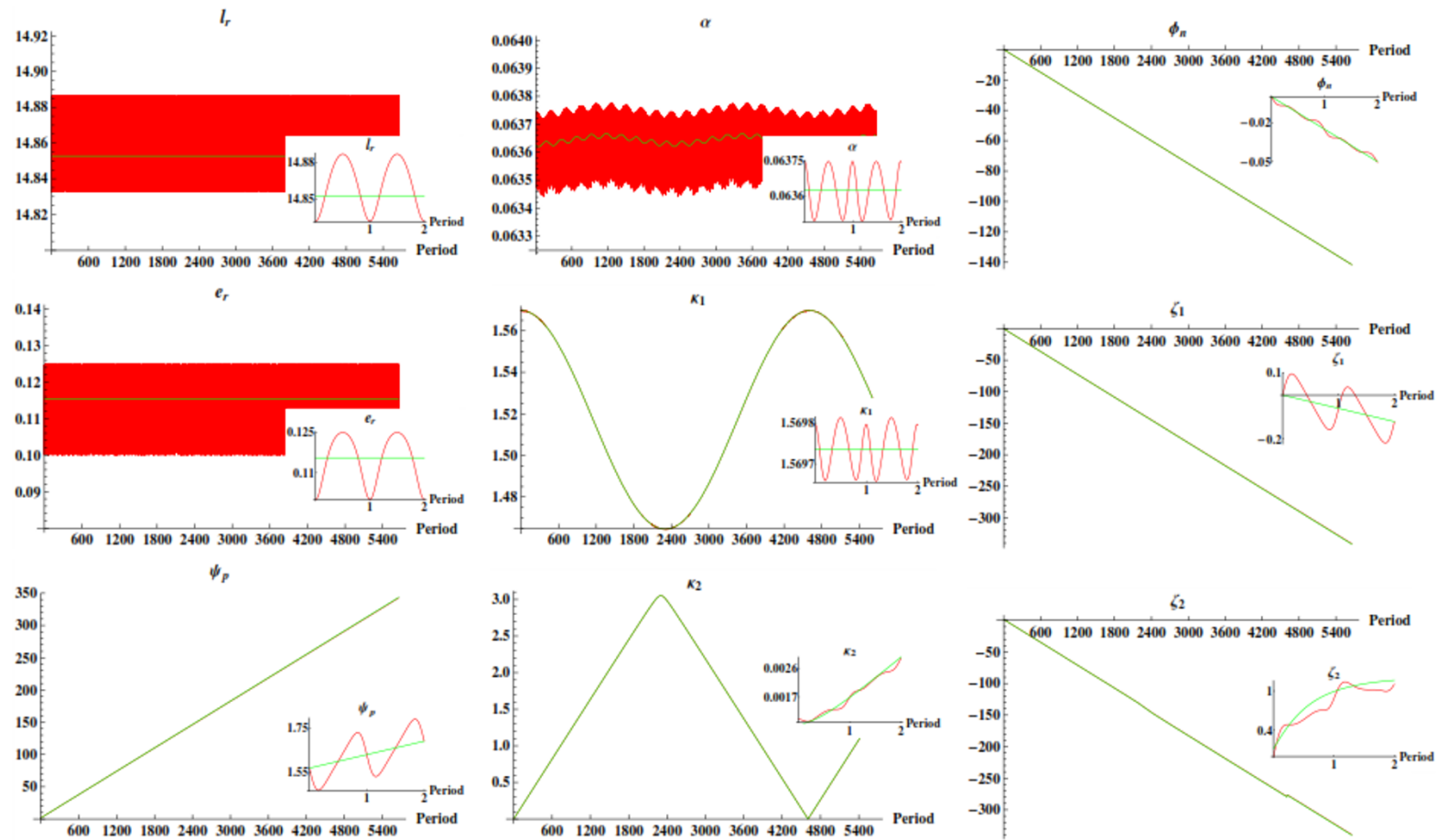


**Figure 1.** From the upper left diagram to the lower right, the evolutions of  $l_r, e_r, \alpha, \phi_n, \psi_p, \kappa_i, \zeta_i$  ( $i = 1, 2$ ) are depicted, respectively, as function of the number of orbital periods. They are driven by the secular (green curves) and the instantaneous dynamics (red curves). The parameters and initial conditions are chosen as: total mass  $m = 10M_\odot$ , mass ratio  $\nu = 1.0$ , dimensionless spin parameters  $\chi_1 = 0.95, \chi_2 = 0.05$ , eccentricity  $e_r = 0.1$ , spin polar angles  $\kappa_1 = \pi/2, \kappa_2 = 0.001$ , spin azimuthal angles  $\zeta_1 = 0, \zeta_2 = 0$ , longitude of the ascending node  $\phi_n = 0$ . The shape variables  $l_r, e_r$  gives the post-Newtonian parameter  $\varepsilon = (1 + e_r) l_r^2$ .

In the presented case, one of the spins is much smaller than the other  $\chi_2 = 19\chi_1$ . The initial data was chosen with the dominant spin perpendicular to  $\hat{\mathbf{L}}_N$ . As the middle figures in the last two columns on Figure 1 show, the dominant spin undergoes a rotation about the direction of  $\hat{\mathbf{L}}_N$ , and it remains almost perpendicular to  $\hat{\mathbf{L}}_N$  during the evolution. However the smaller spin ventures from pole to pole (defined by  $\hat{\mathbf{L}}_N$ ). This feature was initially identified in [47] as spin flip-flop. Other configurations were discussed as either spin instabilities [48] or unstable flip-flops [49] or generic flip-flops [50]. These results are easily reproduced by the derived secular dynamics [46]. In addition, the ascending node  $\hat{\mathbf{I}}$  rotates around the total angular momentum. In the instantaneous plane of the motion  $\mathbf{A}_N$  rotates around  $\mathbf{L}_N$ . Since  $\cos \alpha > 0$ , both rotations are anticlockwise from the direction of  $\hat{\mathbf{J}}$ .

The secular evolutions of the spins directions are shown on Figure 2 in the frame determined by  $\hat{\mathbf{A}}_N$ ,  $\hat{\mathbf{L}}_N \times \hat{\mathbf{A}}_N$  and  $\hat{\mathbf{L}}_N$ . The motion of the dominant spin (red), is almost a pure rotation around  $\hat{\mathbf{L}}_N$ . This rotation is clockwise about  $\hat{\mathbf{L}}_N$ . The orbit of the tip of the smaller spin (the blue curve) encircles the unit sphere several times on a helical path from North pole to South pole and vice-versa. The direction of the movement is clockwise about  $\hat{\mathbf{L}}_N$  under the full evolution.

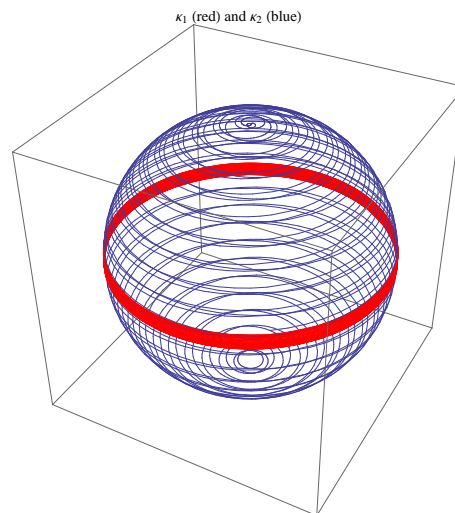


**Figure 2.** The evolutions of the unit spin vectors in the frame determined by  $\hat{\mathbf{A}}_N$ ,  $\hat{\mathbf{L}}_N \times \hat{\mathbf{A}}_N$  and  $\hat{\mathbf{L}}_N$ . The movement of the dominant spin  $\hat{\mathbf{S}}_1$  and the smaller spin  $\hat{\mathbf{S}}_2$  are depicted in red and blue, respectively.

### 3. Conclusions

The dynamics of a spinning compact binary is complicated enough, even at a conservative level, as given in detail in [40]. Hence, for processes occurring over the precessional time-scale of the spin and orbital angular vectors, the details of the orbital dynamics could be suppressed by a proper averaging over the orbital period. This process gives a simpler, yet also complicated secular dynamics of the set of angles characterizing the relative orientations of the vectors involved (spin and Euler angles). This dynamics has been derived in [46] in the form of an autonomous closed system of first-order differential equations for the pairs of polar and azimuthal angles of the spins and orbital angular momentum vector together with the periastron angle. These variables are subject to two algebraic constraints.

The effects occurring on this time-scale are easier to monitor in this system. Indeed, we explored the possibility to analyze the occurrence and extent of the spin flip-flop effect by studying this system analytically over the entire parameter space. Here, we presented one example of this analysis.

The time-scale over which radiation-reaction has a significant effect (this is the gravitational radiation time-scale) depends on the value of the PN parameter. At the end of the inspiral, this time-scale becomes short enough such that the orbit evolves dissipatively and the gravitational waves change accordingly. Over the radiation–reaction time-scale the secular dynamics may also be

useful. One of the present authors has been involved in the derivation of the spin-flip effect occurring during the inspiral [51] of a subdominant black-hole into a much larger one, which can explain the formation of the X-shaped radio galaxies [52]. This was based on a much simpler account of the secular dynamics. We plan to supplement the secular dynamics presented here and in [46] with the corresponding leading-order radiation-reaction terms in order to study the spin-flip process more accurately and in greater detail.

**Acknowledgments:** This work was supported by the Hungarian National Research Development and Innovation Office (NKFI) in the form of the grant 123996. The work of Z.K. was supported by the UNKP-17-4 New National Excellence Program of the Ministry of Human Capacities. The work of M.T. was supported by the NTP-NFTÖ-17 National Excellence Program of the Ministry of Human Capacities. L.Á.G. thanks the organizers of the Bolyai-Gauss-Lobachevsky Conference for partial support of his participation.

**Author Contributions:** All authors contributed equally to this work.

**Conflicts of Interest:** The authors declare no conflict of interest.

## References

1. Einstein, A. *Näherungsweise Integration der Feldgleichungen der Gravitation*; Sitzungsberichte der Königlich Preussischen Akademie der Wissenschaften Berlin; Part 1; Wiley-VCH Verlag GmbH & Co. KGaA: Weinheim, Germany, 1916; pp. 688–696.
2. LIGO Scientific Collaboration. Advanced LIGO. *Class. Quantum Grav* **2015**, *32*, 074001.
3. LIGO Scientific Collaboration; Virgo Collaboration. Observation of Gravitational Waves from a Binary Black Hole Merger. *Phys. Rev. Lett.* **2016**, *116*, 061102.
4. LIGO Scientific Collaboration; Virgo Collaboration. GW151226: Observation of Gravitational Waves from a 22-Solar-Mass Binary Black Hole Coalescence. *Phys. Rev. Lett.* **2016**, *116*, 241103.
5. LIGO Scientific Collaboration; Virgo Collaboration. GW170104: Observation of a 50-Solar-Mass Binary Black Hole Coalescence at Redshift 0.2. *Phys. Rev. Lett.* **2017**, *118*, 221101.
6. LIGO Scientific Collaboration; Virgo Collaboration. GW170814: A Three-Detector Observation of Gravitational Waves from a Binary Black Hole Coalescence. *Phys. Rev. Lett.* **2017**, *119*, 141101.
7. Virgo Collaboration. Advanced Virgo: A second-generation interferometric gravitational wave detector. *Class. Quantum Grav* **2014**, *32*, 024001.
8. LIGO Scientific Collaboration; Virgo Collaboration. GW170817: Observation of Gravitational Waves from a Binary Neutron Star Inspiral. *Phys. Rev. Lett.* **2017**, *119*, 161101.
9. Michimura, Y. On behalf of the KAGRA Collaboration, The Status of KAGRA Underground Cryogenic Gravitational Wave Telescope, TAUP2017. Available online: [https://indico.cern.ch/event/606690/contributions/2591396/attachments/1499475/2334708/TAUP2017\\_michimura.pdf](https://indico.cern.ch/event/606690/contributions/2591396/attachments/1499475/2334708/TAUP2017_michimura.pdf) (accessed on 25 January 2018).
10. LIGO-India. Available online: <http://www.gw-indigo.org/tiki-index.php?page=LIGO-India> (accessed on 25 January 2018).
11. Abbott, B.P.; Abbott, R.; Abbott, T.D.; Acernese, F.; Ackley, K.; Adams, C.; Adams, T.; Addesso, P.; Adhikari, R.X.; Adya, V.B.; et al. LIGO Scientific Collaboration, Virgo Collaboration, Fermi Gamma-ray Burst Monitor, and INTEGRAL, Gravitational Waves and Gamma-Rays from a Binary Neutron Star Merger: GW170817 and GRB170817A. *Astrophys. J. Lett.* **2017**, *848*, L13.
12. LIGO Scientific Collaboration; Virgo Collaboration; Fermi GBM; INTEGRAL; IceCube Collaboration; AstroSat Cadmium Zinc Telluride Imager Team; IPN Collaboration; The Insight-Hxmt Collaboration; ANTARES Collaboration; The Swift Collaboration; et al. Multi-messenger Observations of a Binary Neutron Star Merger. *Astrophys. J. Lett.* **2017**, *848*, L12.
13. LIGO Scientific Collaboration; Virgo Collaboration; 1m2H Collaboration; Dark Energy Camera GW-EM Collaboration; DES Collaboration; DLT40 Collaboration; Las Cumbres Observatory Collaboration; VINROUGE Collaboration & MASTER Collaboration. A gravitational-wave standard siren measurement of the Hubble constant. *Nature* **2017**, *551*, 85–88.
14. Lorentz, H.A. Electromagnetic phenomena in a system moving with any velocity smaller than that of light. *Proc. R. Acad. Amst.* **1904**, *6*, 1903–1904.

15. Poincaré, H. Sur la dynamique de l'électron. *Inst. Fr. Acad. Sci. C. R.* **1905**, *140*, 1504–1508.
16. ATLAS Collaboration. Search for electroweak production of supersymmetric states in scenarios with compressed mass spectra at  $\sqrt{s} = 13\text{TeV}$  with the ATLAS detector. *arXiv* **2017**, arXiv:1712.08119.
17. IceCube Collaboration. Search for sterile neutrino mixing using three years of IceCube DeepCore data. *Phys. Rev. D* **2017**, *95*, 112002.
18. LUX Collaboration. Results from a search for dark matter in the complete LUX exposure. *Phys. Rev. D* **2017**, *118*, 021303.
19. Savvidis, I.; Pivovarov, M.J.; Kotthaus, R.; Eleftheriadis, C.; Krčmar, M.; García, J.A.; Villar, J.; Riege, H.; Ferrer-Ribas, E.; Rashba, T.; et al. CAST search for sub-eV mass solar axions with  $^3\text{He}$  buffer gas. *Phys. Rev. Lett.* **2011**, *107*, 261302.
20. Choudhury, D.; Ghosh, K. Bounds on Universal Extra Dimension from LHC Run I and II data. *arXiv* **2016**, arXiv:1606.04084.
21. Alcock, C.; Allsman, R.A.; Alves, D.R.; Axelrod, T.S.; Becker, A.C.; Bennett, D.P.; Cook, K.H.; Dalal, N.; Drake, A.J.; Freeman, K.C.; et al. The MACHO Project: Microlensing Results from 5.7 Years of Large Magellanic Cloud Observations. *Astrophys. J.* **2000**, *542*, 281–307.
22. María Ezquiaga, J.; Zumalacárregui, M. Dark Energy after GW170817: dead ends and the road ahead. *Phys. Rev. Lett.* **2017**, *119*, 251304.
23. LIGO Scientific Collaboration; Virgo Collaboration. Tests of General Relativity with GW150914. *Phys. Rev. Lett.* **2016**, *116*, 221101.
24. Damour, T.; Deruelle, N. General relativistic celestial mechanics of binary systems. I. The post-Newtonian motion. *Ann. Inst. Henri Poincaré* **1985**, *43*, 107–132.
25. Kidder, L.E.; Will, C.M.; Wiseman, A.G. Spin effects in the inspiral of coalescing compact binaries. *Phys. Rev. D* **1993**, *47*, R4183.
26. Kidder, L.E. Coalescing binary systems of compact objects to (post) $^{5/2}$ -Newtonian order. V. Spin effects. *Phys. Rev. D* **1995**, *52*, 821.
27. Rieth, R.; Schäfer, G. Spin and tail effects in the gravitational-wave emission of compact binaries. *Class. Quantum Gravity* **1997**, *14*, 2357–2380.
28. Gergely, L.Á.; Perjés, Z.I.; Vasúth, M. Spin effects in gravitational radiation backreaction III. Compact binaries with two spinning components. *Phys. Rev. D* **1998**, *58*, 124001.
29. Gergely, L.Á. Spin-spin effects in radiating compact binaries. *Phys. Rev. D* **2000**, *61*, 024035.
30. Gergely, L.Á. Second post-Newtonian radiative evolution of the relative orientations of angular momenta in spinning compact binaries. *Phys. Rev. D* **2000**, *62*, 024007.
31. Poisson, E. Gravitational waves from inspiraling compact binaries: The quadrupole-moment term. *Phys. Rev. D* **1998**, *57*, 5287–5290.
32. Gergely, L.Á.; Keresztes, Z. Gravitational radiation reaction in compact binary systems: Contribution of the quadrupole-monopole interaction. *Phys. Rev. D* **2003**, *67*, 024020.
33. Gergely, L.Á. Spinning compact binary inspiral: Independent variables and dynamically preserved spin configurations. *Phys. Rev. D* **2010**, *81*, 084025.
34. Gergely, L.Á. Spinning compact binary inspiral. II. Conservative angular dynamics. *Phys. Rev. D* **2010**, *82*, 104031.
35. Apostolatos, T.A.; Cutler, C.; Sussman, G.J.; Thorne, K.S. Spin-induced orbital precession and its modulation of the gravitational waveforms from merging binaries. *Phys. Rev. D* **1994**, *49*, 6274–6297.
36. Racine, É. Analysis of spin precession in binary black hole systems including quadrupole-monopole interaction. *Phys. Rev. D* **2008**, *78*, 044021.
37. González, J.A.; Sperhake, U.; Brüggmann, B.; Hannam, M.; Husa, S. Maximum Kick from Nonspinning Black-Hole Binary Inspiral. *Phys. Rev. Lett.* **2007**, *98*, 091101.
38. Campanelli, M.; Lousto, C.O.; Zlochower, Y.; Merritt, D. Maximum Gravitational Recoil. *Phys. Rev. Lett.* **2007**, *98*, 231102.
39. Lousto, C.O.; Zlochower, Y. Hangup Kicks: Still Larger Recoils by Partial Spin/Orbit Alignment of Black-Hole Binaries. *Phys. Rev. Lett.* **2011**, *107*, 231102.
40. Gergely, L.Á.; Keresztes, Z. Spinning compact binary dynamics and chameleon orbits. *Phys. Rev. D* **2015**, *91*, 024012.
41. Barker, B.M.; O'Connell, R.F. Derivation of the Equations of Motion of a Gyroscope from the Quantum Theory of Gravitation. *Phys. Rev. D* **1970**, *2*, 1428–1435.

42. Barker, B.M.; O'Connell, R.F. Gravitational two-body problem with arbitrary masses, spins, and quadrupole moments. *Phys. Rev. D* **1975**, *12*, 329.
43. Kesden, M.; Gerosa, D.; O'Shaughnessy, R.; Berti, E.; Sperhake, U. Effective potentials and morphological transitions for binary black-hole spin precession. *Phys. Rev. Lett.* **2015**, *114*, 081103.
44. Gerosa, D.; Kesden, M.; Sperhake, U.; Berti, E.; O'Shaughnessy, R. Multi-timescale analysis of phase transitions in precessing black-hole binaries. *Phys. Rev. D* **2015**, *92*, 064016.
45. Chatziioannou, K.; Klein, A.; Cornish, N.; Yunes, N. Analytic gravitational waveforms for generic precessing compact binaries. *arXiv* **2016**, arXiv:1606.03117.
46. Tápai, M.; Keresztes, Z.; Gergely, L.Á. Secular precessing compact binary dynamics, spin and orbital angular momentum flip-flops. *arXiv* **2015**, arXiv:1609.05915.
47. Lousto, C.O.; Healy, J. Flip-flopping binary black holes. *Phys. Rev. Lett.* **2015**, *114*, 141101.
48. Gerosa, D.; Kesden, M.; O'Shaughnessy, R.; Klein, A.; Berti, E.; Sperhake, U.; Trifirň, D. Precessional instability in binary black holes with aligned spins. *Phys. Rev. Lett.* **2015**, *115*, 141102.
49. Lousto, C.O.; Healy, J. Unstable flip-flopping spinning binary black holes. *Phys. Rev. D* **2016**, *93*, 124074.
50. Lousto, C.O.; Healy, J.; Nakano, H. Spin flips in generic black hole binaries. *Phys. Rev. D* **2016**, *93*, 044031.
51. Gergely, L.Á.; Biermann, P.L. The spin-flip phenomenon in supermassive black hole binary mergers. *Astrophys. J.* **2009**, *697*, 1621.
52. Gopal-Krishna; Biermann, P.L.; Gergely, L.Á.; Wiita, P.J. On the origin of X-shaped radio galaxies. *Res. Astron. Astrophys.* **2012**, *12*, 127–146.



© 2018 by the authors. Licensee MDPI, Basel, Switzerland. This article is an open access article distributed under the terms and conditions of the Creative Commons Attribution (CC BY) license (<http://creativecommons.org/licenses/by/4.0/>).